

Programmable actuating systems based on swimming fiber robot

Hao Sun^{a†}, Meng Liao^{a,c†}, Jianfeng Li^a, Chao Zhou^b, Jue Deng^a, Xuemei Fu^a, Songlin Xie^a, Bo Zhang^a, Yizheng Wu^b, Bingjie Wang^{a,c}, Xuemei Sun^{a,c}, Huisheng Peng^{a,c}*

^aState Key Laboratory of Molecular Engineering of Polymers and Department of Macromolecular Science, Fudan University, Shanghai 200438, China.

^bState Key Laboratory of Surface Physics, Department of Physics and Collaborative Innovation Center of Advanced Microstructures, Fudan University, Shanghai 200438, China.

^cLaboratory of Advanced Materials, Fudan University, Shanghai 200438, China.

†These authors contributed equally to this work

*Corresponding author. E-mail: penghs@fudan.edu.cn (Huisheng Peng)

This PDF file includes:

Supplementary Notes S1 to S9 (Pages S2-S6)

Supplementary Figures S1 to S12 (Pages S7-S18)

Supplementary Table S1 (Page S19)

Captions for Supplementary Movie S1 to S9 (Page S20)

Supplementary References (Page S21)

Supplementary Notes

1. Synthesis of Fe₃O₄ nanoparticles

Fe₃O₄ nanoparticles were synthesized *via* a co-precipitation method. FeCl₂·4H₂O (5.6 mmol) and FeCl₃·6H₂O (11.2 mmol) were dissolved in deionized water (150 mL) in a 250 mL three-neck flask. The resulting mixture solution was then heated to 50 °C with vigorous stirring under a nitrogen atmosphere. Aqueous ammonia solution (25%, 12.5 mL) was rapidly added to the mixture with an obvious color change to black. The reaction solution was then cooled down to room temperature after reaction for 30 min. After washing with diluted hydrochloric acid and deionized water, aqueous Fe₃O₄ dispersion was obtained.

2. Preparation of MWCNT fibers

MWCNT fibers were dry-spun from spinnable MWCNT arrays. To prepare spinnable MWCNT arrays, Fe (1.2 nm)/Al₂O₃ (5 nm) were deposited on a silicon wafer to serve as the catalyst. Ethylene was used as carbon source with a flowing rate of 90 sccm, and a mixture of Ar (480 sccm) and H₂ (30 sccm) was used as the carrier gas with a deposition temperature of 750 °C. The thickness of spinnable MWCNT array was ~200 μm. MWCNT fibers were spun from spinnable MWCNT arrays with the same width of ~7 mm using a manual spinning machine. The fiber diameter can be controlled by varying the layer number of MWCNT sheet.

3. Characterization

The structures and morphologies of the actuating system were characterized by scanning electron microscopy (SEM, Hitachi, FE-SEM S-4800 operated at 1 kV). Electrochemical deposition was conducted on a CHI 660D electrochemical workstation.

The photographs and videos were taken by a digital camera (SONY A6000, Japan). The movements of SFRs under magnetic field were conducted in a magnetic field with a maximum strength of 2.7 kOe along the arbitrary in-plane was applied by a vector magnet.

4. Calculation of Pt weight percentage

The mass of deposited Pt can be calculated from the equation of $m_1 = (Q \times M) / (n \times F)$, where Q , M , n and F correspond to the charge quantity changing, molecular weight of Pt, specific valence change for Pt during electrodeposition process and Faraday constant, respectively. The weight of aligned MWCNT fiber was calculated from the equation of $m_2 = n \times \rho_a \times S$, where n , ρ_a and S correspond to the sheet number, areal density and area of MWCNT sheet, respectively. The areal density of MWCNT sheet was $\sim 1.41 \mu\text{g}\cdot\text{cm}^{-2}$. The Pt weight percentage in MWCNT/Pt hybrid fiber can be thus calculated from the equation of $\eta = m_1 / (m_1 + m_2)$.

5. Derivation of angular speed

At the steady state, the net driving force produced by the reaction should be balanced by the drag force due to the friction, i.e.,

$$\sum_{k \in Pt} f_0 \mathbf{u}_k - \sum_k (\mathbf{v}_0 + \boldsymbol{\omega} \times \mathbf{r}_k) \zeta = 0.$$

where f_0 is the force produced by a length element, \mathbf{u}_k denotes the direction of the driving force of the k^{th} element, the summation on the left only sums over the length elements covered by Pt, \mathbf{v}_0 is the velocity of the mass center of the rigid body, $\boldsymbol{\omega}$ is the angular speed of the body, \mathbf{r}_k is the distance of the k^{th} element to the mass center and ζ is the friction coefficient of every length element. Because $\sum_k \mathbf{r}_k = 0$, so the above equation is reduced to

$$\mathbf{v}_0 = \mathbf{F}_{dr} / N\zeta \quad (1)$$

where \mathbf{F}_{dr} is the net driving force and N is the total number of the length element. Similarly, the torque produced by the reaction must be also balanced by the torque produced by the drag force of the friction which gives:

$$\sum_{k \in Pt} f_0 \mathbf{u}_k \times \mathbf{r}_k - \sum_k \boldsymbol{\omega} \times \mathbf{r}_k \times \mathbf{r}_k \zeta = 0 \quad (2)$$

The angular speed can be obtained by solving the above equation,

$$\boldsymbol{\omega} = \zeta^{-1} \left(\sum_k \mathbf{r}_k \mathbf{r}_k^T - \mathbf{I} \sum_k |\mathbf{r}_k|^2 \right)^{-1} \boldsymbol{\tau}_{dr} \quad (3)$$

where \mathbf{r}_k^T is the transpose of the row vector \mathbf{r}_k and \mathbf{I} is the identity matrix.

6. Dependence of angular speed on detached diameter of released bubble

According to the previous work by Gibbs *et al.*,¹ the angular speed depends on the concentration (c) of H_2O_2 and the detached size or diameter (D) of the bubble by the Langmuir isotherm type of function with P_1 and P_2 two parameters related to the specific system in question. In this work, $P_1 = 1.0$ and $P_2 = 0.02$. The dependence of the detached diameter of the bubble on the concentration of H_2O_2 can be determined by fitting the experimental data using a quadratic function $D(c) = (235.7c^2 + 0.9286c + 28.9)\mu\text{m}$. It is expected that the dependence of the angular speed on the weight percentage of Pt follows the same relationship in Figure 2e.

7. Typical fiber module: a linear rod half covered with Pt

Consider a linear rod with the length L where half of the rod was covered with Pt. The velocity of the mass can be easily computed using eq. (1) as

$$\mathbf{v}_0 = \frac{f_0}{2\zeta} \mathbf{n} \times \mathbf{u}(t) \quad (4)$$

where \mathbf{n} is the unit vector perpendicular to the water surface and \mathbf{u} denotes the direction of the rod.

By eq. (2)

$$\zeta\omega\int_0^{a/2} x^2 dx = f_0\int_0^{a/2} x dx$$

and we have

$$\omega = \frac{3f_0([H_2O_2])}{2\zeta a} . \quad (5)$$

Therefore, at any instant, the rod will revolve around the mass center of the rod with the angular speed given by eq. (5) but the mass center will also move with the velocity given by eq. (4). These two motions render the mass center to circulate around a point with radius r_c . After a short period, the mass center will move with a distance $\Delta s = \Delta t v_0 = r_c \Delta \theta = r_c \omega \Delta t$, which gives $r_c = v_0 / \omega = a / 3$. Herein the linear rod will circulate around a fixed point, which locates at the $a / 6$ of the uncovered side of the rod, with the angular speed of $3f_0 / 2a\zeta$.

8. Rotation of triangular shape in Figure 4e

Then we consider the rotation of triangular rods (Figure 4e). Because the water surface bounded by the triangle will move or rotate with the triangle, so this motion will also produce some drag forces preventing the triangle from moving or rotating. For simplicity, we assume the friction coefficient of the bounded water is γ .

Obviously, the net driving torque can be calculated below,

$$\boldsymbol{\tau}_{dr} = \sum_{k \in Pt} f_0 \mathbf{u}_k \times \mathbf{r}_k = 3f_0 \int_0^{a/2} (0, 0, -x) dx = (0, 0, -1) \frac{3f_0 a^2}{8} \quad (6)$$

or $\tau_{dr} = \frac{3f_0 a^2}{8}$. On the other hand, the torque due to the drag forces can be obtained as

follow,

$$\begin{aligned} \tau_{drag} &= 6[\gamma \int_{y=0}^{\sqrt{3}a/6} \int_{x=0}^{a/2-\sqrt{3}y} (x^2 + (y - \frac{\sqrt{3}a}{6})^2) dx dy + \zeta \int_0^{a/2} ((\sqrt{3}a/6)^2 + x^2) dx] \omega \\ &= (\frac{\sqrt{3}\gamma a^4}{48} + \frac{\zeta a^3}{2}) \omega \end{aligned} \quad (7)$$

Eqs. (6) and (7) lead to

$$\omega = \frac{f_0([H_2O_2])}{a\left(\frac{4}{3}\zeta + \frac{a\gamma}{6\sqrt{3}}\right)} \quad (8)$$

The two friction coefficients can be determined by matching the experimental data and they are $\frac{\zeta}{f_0} = 0.046\text{s/mm}$ and $\frac{\gamma}{f_0} = 0.489\text{s/mm}^2$. By this parameter setting, it is about 6.27s per cycle which is very close to that measured value in experiment (6s/cycle).

9. Linear movement of squared shape in Figure 4g

The net driving force is obviously $F_{dr} = f_0 a$ while the total drag force is

$$F_{drag} = (a^2\gamma' + 4a\zeta)v_0$$

where the first term on the right accounts for the friction force due to the translational motion of the bounded water by the rods. So we have

$$v_0 = \frac{f_0}{a\gamma' + 4\zeta}$$

Similarly, the friction coefficient (translational motion) can be also determined by matching the experimental data and it is $\frac{\gamma'}{f_0} = 0.0855\text{s/mm}^2$ ($\frac{\zeta}{f_0} = 0.046\text{s/mm}$). By this parameter setting, it is found that the shape will move about a distance of $a = 3.5\text{mm}$ within 1.69 s which is also close to that measured value in experiment (1.2 s/a).

Supplementary Figures

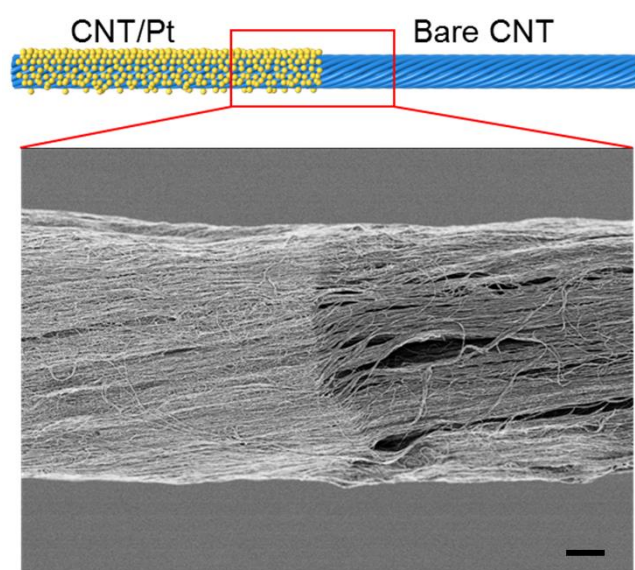


Figure S1. Schematic illustration and the corresponding SEM image of the interface between bare MWCNT and Pt-deposited MWCNT sections. Scale bar, 2 μm .

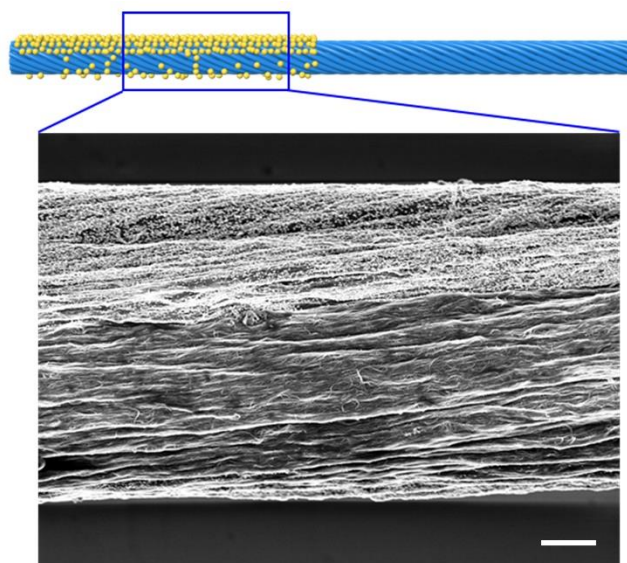


Figure S2. Schematic illustration and the corresponding SEM image of the heterosectional Pt deposition. Scale bar, 2 μm .

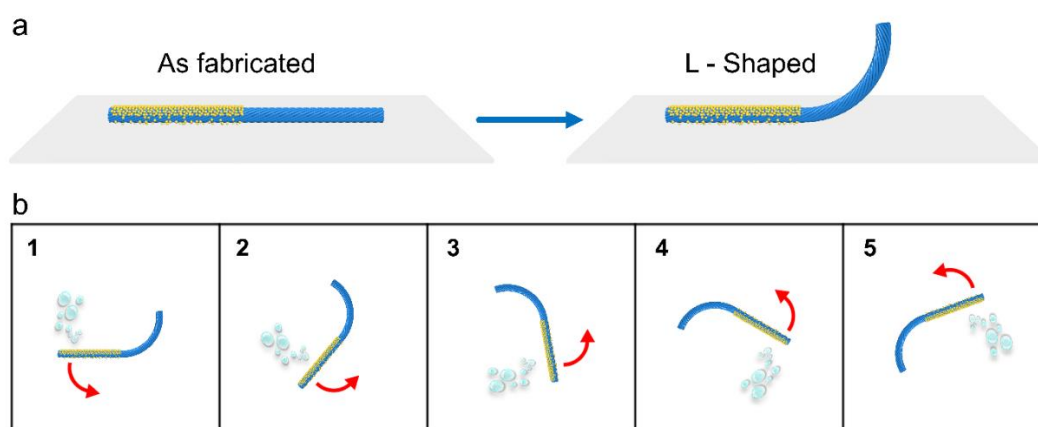


Figure S3. **a**, Schematic illustration to the preparation of an L-shaped SFR. **b**, Schematic illustration of the rotation trajectory of the SFR at **a**. The rotating direction indicated that the propelling force was generated by the side with more Pt deposition. The reconfigured images were obtained from Movie S3.

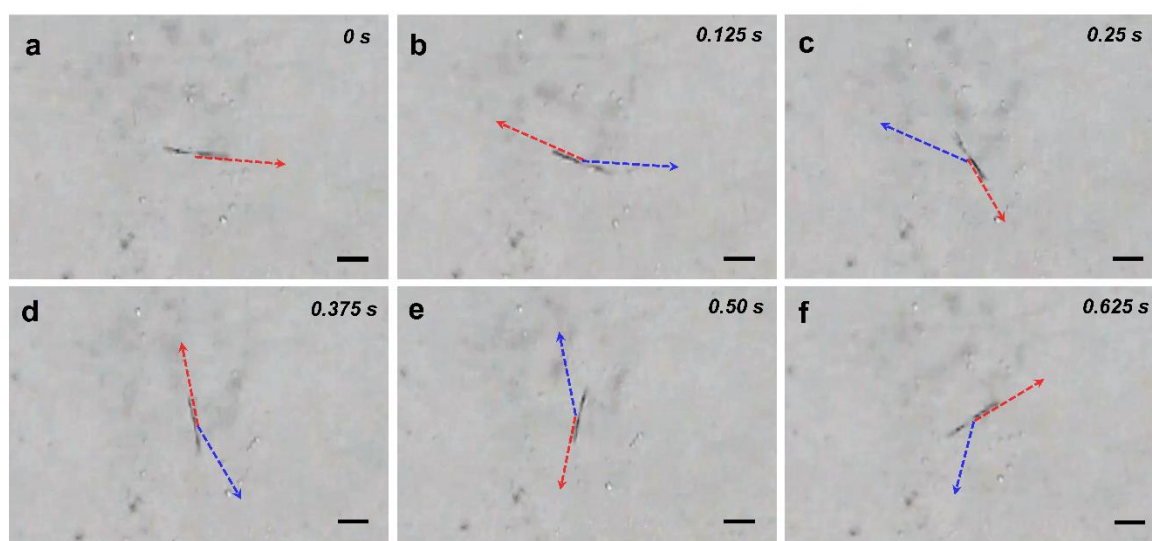


Figure S4. Optical images of an SFR rotating in aqueous H_2O_2 solution. Each two neighbouring images shared the time interval of 0.125 s. The red arrows indicate the current sites of SFR in according frames and the blue arrows at **b-f** indicate the original sites of SFR in the former frame. Scale bar, 1 mm.

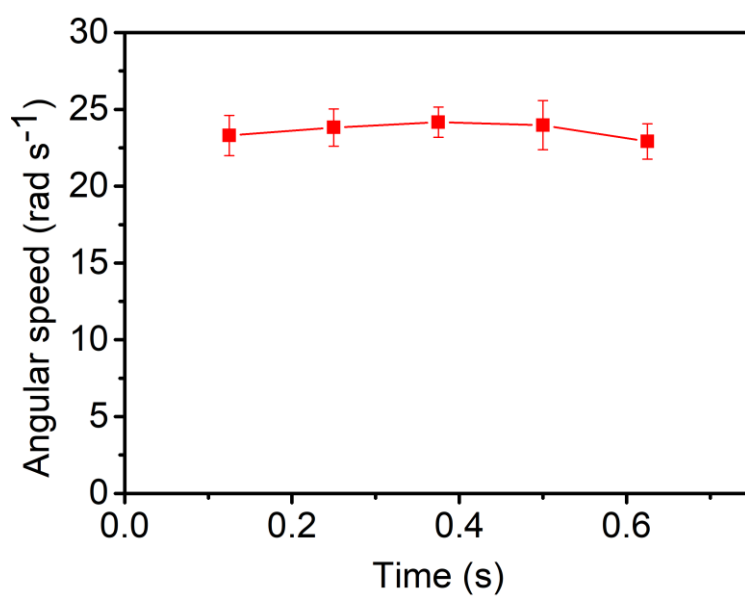


Figure S5. Angular speeds in 5 continuous moments of a rotary circle.

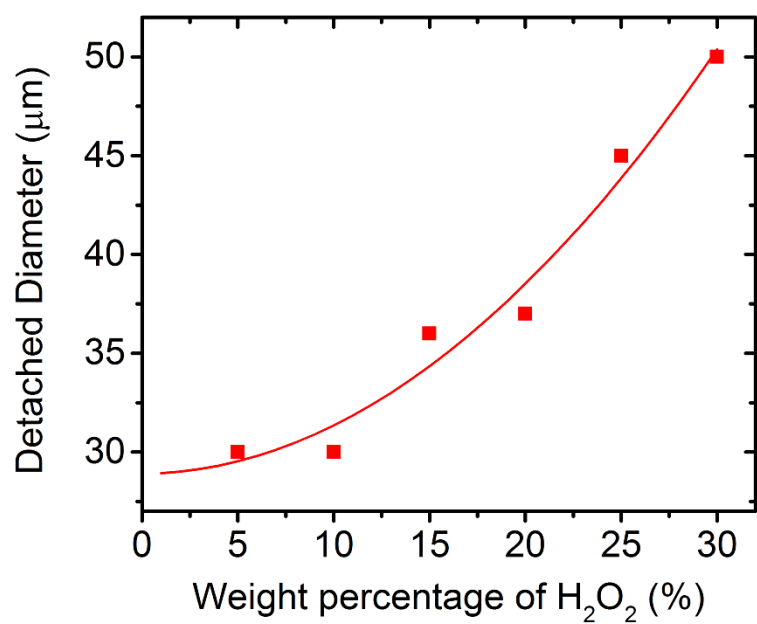


Figure S6. Dependence of detached bubble diameter from SFR on weight percentage of H₂O₂ under a steady condition.

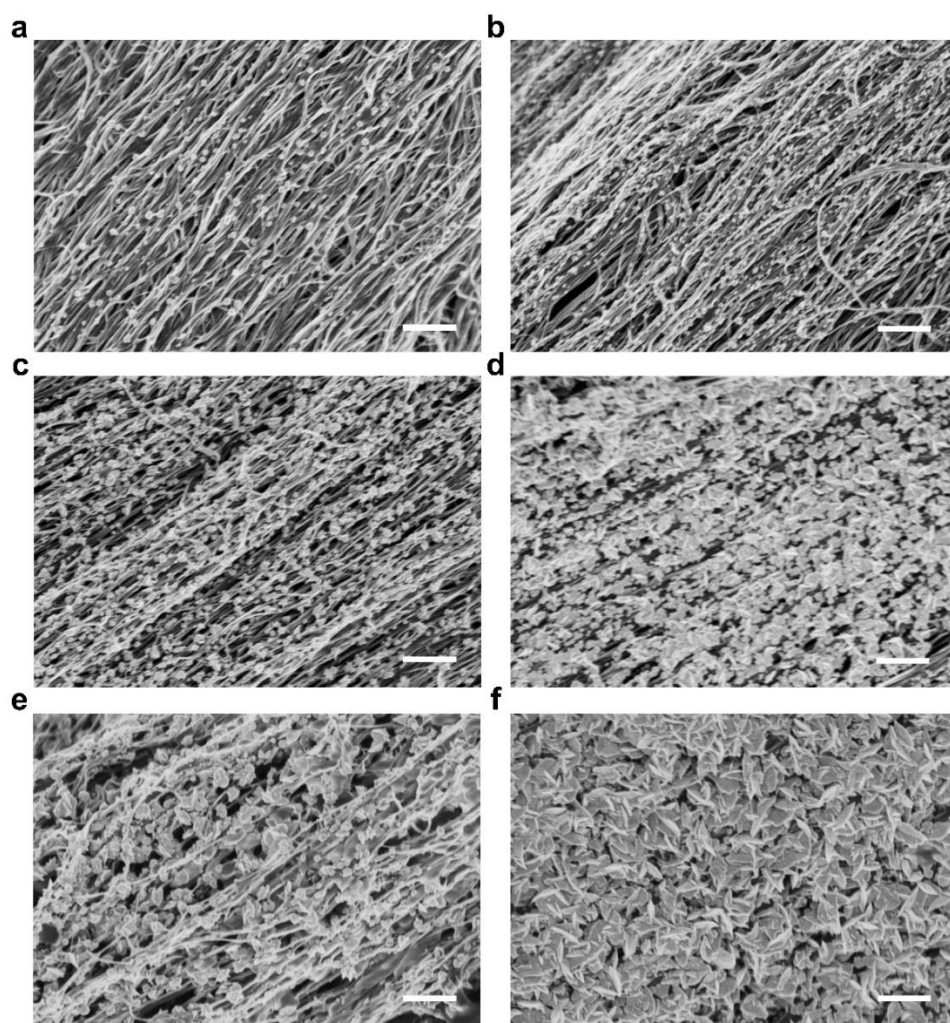


Figure S7. SEM images of Pt-deposited section with increasing platinum weight percentages of 12% (a), 32.5% (b), 48.5% (c), 57.7% (d), 68.5% (e) and 74.2% (f). Scale bars, 500 nm.

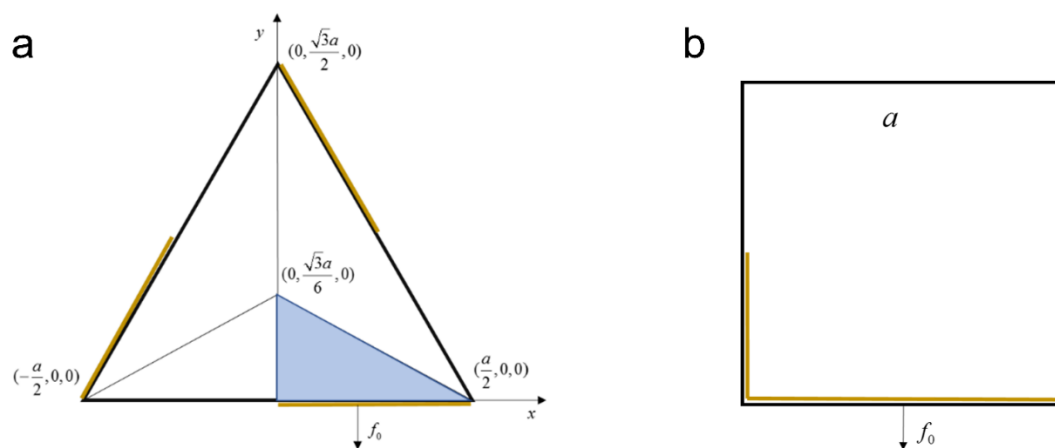


Figure S8. Typical construction diagrams showing the mechanical analysis of rotary (a) and translational (b) modular microrobots.







Structure	Simulation equation	Simulation	Experiment
	$\omega = \frac{3f_0([H_2O_2])}{a(\frac{4\zeta}{3} + \frac{\sqrt{3}a\gamma}{6})}$	3.39 s / C	3.5 s / C
	$\omega = \frac{f_0([H_2O_2])(\frac{3}{8} - \frac{\cos\theta}{3})}{a[(\frac{14}{9} + \frac{26}{9}\theta - \frac{2}{3}\cos\theta - \frac{8}{3}\sin\theta)\zeta + (\frac{17}{18}\theta - \frac{8}{9}\sin\theta)a\gamma]}$	6.37 s / C	2.1 s / C
	$\omega = \frac{f_0([H_2O_2])}{a(\frac{4}{3}\zeta + \frac{a\gamma}{6\sqrt{3}})}$	6.27 s / C	6.1 s / C
	$v = \frac{f_0([H_2O_2])}{(6\zeta + \frac{\sqrt{3}a\gamma}{2})}$	3.27 s / A	3.0 s / A
	$v = \frac{f_0([H_2O_2])}{(4\zeta + a\gamma)}$	1.69 s / A	1.2 s / A
	$v = \frac{f_0([H_2O_2])(\sin\theta_1 + \sin\theta_2)}{8\zeta}$	1.99 s / A	2.1 s / A

Figure S9. Experimental and simulation studies of representative modular microrobots. C represents the angular speed per rotating circle. A represents the translation velocity per body length.

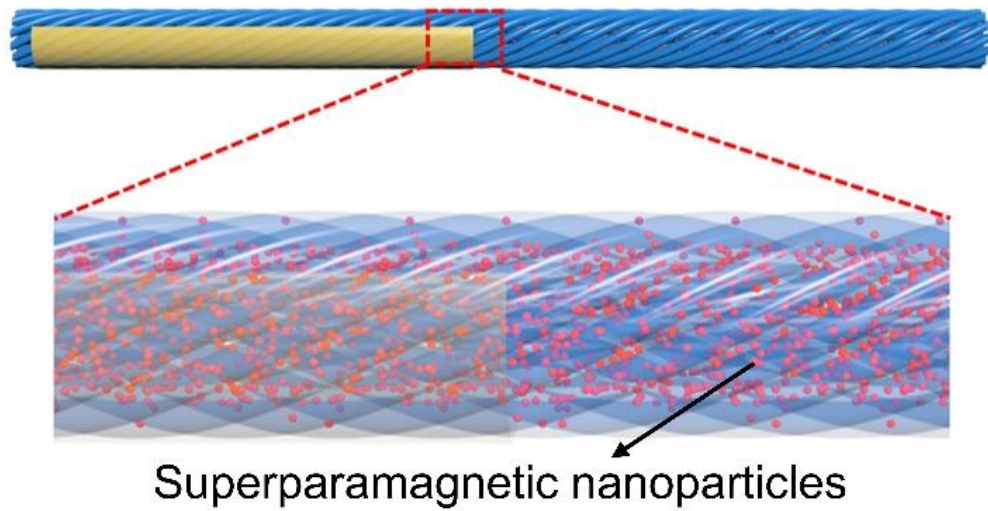


Figure S10. **a**, Schematic illustration to a Fe_3O_4 -incorporated SFR at system level. **b** and **c**, SEM images of Fe_3O_4 -incorporated SFR at low and high magnifications, respectively. The red arrows at **c** indicate the presence of Fe_3O_4 superparamagnetic nanoparticles. Scale bars, 10 μm at **b** and 500 nm at **c**.

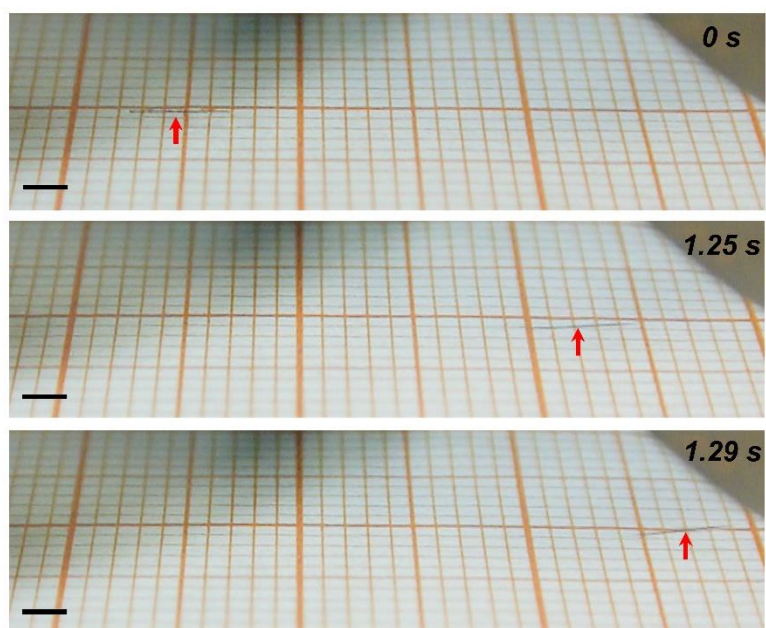


Figure S11. The movement of a Fe_3O_4 -incorporated SFR (indicated by red arrows) in deionized water under a magnetic field of 2500 Oe. Scale bars, 2 mm.

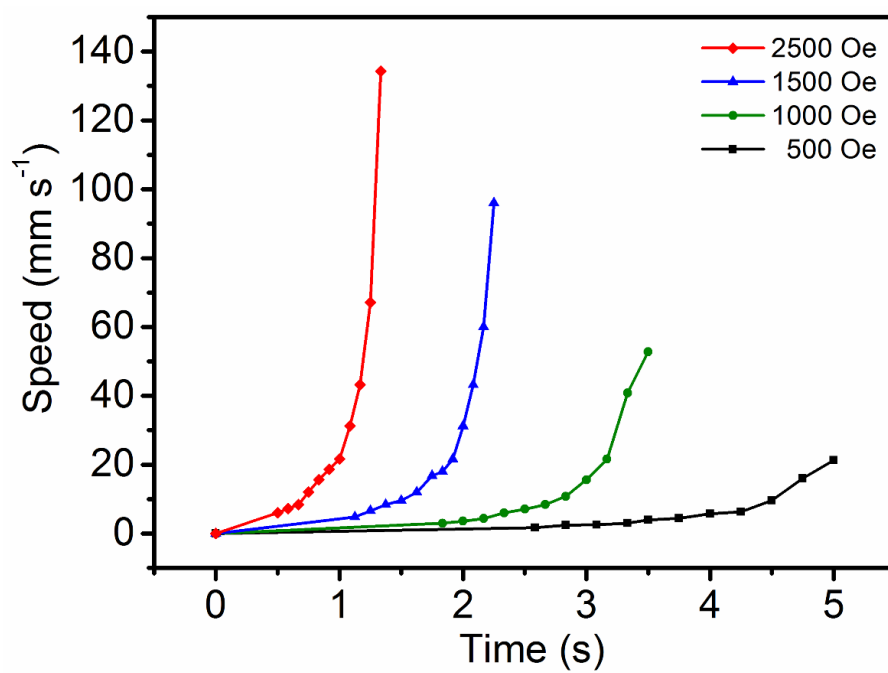


Figure S12. Dependence of the speed on acceleration time under increasing magnetic fields from 500 to 2500 Oe.

Supplementary Table

Table S1. Comparison of actuating systems in our work with reported ones in concern of different movement rates and the assembly potential towards more complex microrobotic systems.

Ref	Architecture	Motion mode	Angular speed (rpm)	Translational speed ($\mu\text{m s}^{-1}$)	Driving source	Assembly
S2	Particle	Rotation and translation	6.67	1162.8	Electric field	1 plate-like primary assembly, rotation and translation movements
S3	Gear	Rotation	300	-	Light field	-
S4	Rotor	Rotation	0.32	-	Chemical fuel and electric field	1 gear-like primary assembly, rotation movement
S4	Sphere	Translation	-	512	Chemical fuel and electric field	-
S5	Helix	Translation	-	55	Magnetic field and bioenergy	-
S6	Hoverboard-like	Rotation	4.29	-	Light field	-
S6	Cone	Translation	-	3.46×10^4	Light field	-
S7	Tadpole-like	Rotation and translation	200	120	Acoustic field	-
S8	Wire	Translation	-	200	Chemical fuel	-
S9	Wire	Translation	-	150	Chemical fuel	-
S10	Tube	Translation	-	78	Magnetic field	-
S11	Rod	Rotation	400	-	Chemical fuel	-
S12	Rod	Rotation	23.72	-	Chemical fuel	-
S13	Rod	Translation	-	2.1	Light field	-
S14	Rod	Rotation and translation	2.87	5	Light field and chemical fuel	-
This work	Rod	Rotation and translation	213.1	1.34×10^5	Chemical fuel and magnetic field	20 different primary assemblies with rotation and translation movements; 2 secondary assemblies with switchable rotation and translation modes

Captions for Supplementary Movies

Movie S1. Typical rotation of a swimming fiber robot (74.2 wt% Pt and 4 mm-long in 30% H₂O₂).

Movie S2. Swimming fiber robot with a high angular speed (74.2 wt% Pt and 2 mm-long in 30% H₂O₂).

Movie S3. Typical rotation of an L-shaped SFR, demonstrating that the propelling force was generated from the denser Pt coated side.

Movie S4. Rotation of a Pt modified graphene fiber (50.4 wt% Pt and 4 mm-long in 30% H₂O₂).

Movie S5. Motion trajectory of a Fe₃O₄-incorporated SFR in a 2500 Oe magnetic field.

Movie S6. SFR simultaneously driven by sources of chemical fuel and magnetic field.

Movie S7. Representative examples of programmable actuating system.

Movie S8. Motion mode-switchable actuating system.

Movie S9. Fish-liked actuating system for cargo transporting application.

Supplementary References

- (1) J. G. Gibbs, Y. P. Zhao, *Small* **2009**, *5*, 2304-2308.
- (2) S. T. Chang, V. N. Paunov, D. N. Petsev, O. D. Velev, *Nat. Mater.* **2007**, *6*, 235-240.
- (3) C. Maggi, F. Saglimbeni, M. Dipalo, F. D. Angelis, R. D. Leonardo, *Nat. Commun.* **2015**, *6*, 7855-7859.
- (4) G. Loget, A. Kuhn, *Nat. Commun.* **2011**, *2*, 535-540.
- (5) M. Medinasánchez, L. Schwarz, A. K. Meyer, F. Hebenstreit, O. G. Schmidt, *Nano Lett.* **2016**, *16*, 555-561.
- (6) F. Meng, W. Hao, S. Yu, R. Feng, Y. Liu, F. Yu, P. Tao, W. Shang, J. Wu, C. Song, *J. Am. Chem. Soc.* **2017**, *139*, 12362-12365.
- (7) M. Kaynak, A. Ozcelik, A. Nourhani, P. E. Lammert, V. H. Crespi, T. J. Huang, *Lab Chip* **2017**, *17*, 395-400.
- (8) R. Laocharoensuk, J. Burdick, J. Wang, *ACS Nano* **2008**, *2*, 1069-1075.
- (9) U. K. Demirok, R. Laocharoensuk, K. M. Manesh, J. Wang, *Angew. Chem., Int. Ed.* **2008**, *120*, 9489-9491.
- (10) S. Sanchez, A. A. Solovev, S. M. Harazim, O. G. Schmidt, *J. Am. Chem. Soc.* **2011**, *133*, 701-703.
- (11) Y. Wang, S. T. Fei, Y. M. Byun, P. E. Lammert, V. H. Crespi, A. Sen, T. E. Mallouk, *J. Am. Chem. Soc.* **2009**, *131*, 9926-9927.
- (12) L. Qin, M. J. Banholzer, X. Xu, L. Huang, C. A. Mirkin, *J. Am. Chem. Soc.* **2007**, *129*, 14870-14871.
- (13) S. Palagi, A. G. Mark, Y. R. Shang, M. Kai, Q. Tian, Z. Hao, C. Parmeggiani, D. Martella, A. Sanchezcastillo, N. Kapernaum, *Nat. Mater.* **2016**, *15*, 647-654.
- (14) B. Dai, J. Wang, Z. Xiong, X. Zhan, W. Dai, C. C. Li, S. P. Feng, J. Tang, *Nat. Nanotechnol.* **2016**, *11*, 1087-1092.